

## Article

# Time- and Sex-Dependent Effects of Fingolimod Treatment in a Mouse Model of Alzheimer's Disease

Pablo Bascuñana <sup>1,†</sup>, Mirjam Brackhan <sup>1,2,†</sup>, Luisa Möhle <sup>1</sup>, Jingyun Wu <sup>1</sup>, Thomas Brüning <sup>1</sup>, Ivan Eiriz <sup>1</sup>, Baiba Jansone <sup>3</sup> and Jens Pahnke <sup>1,2,3,4,\*</sup>

<sup>1</sup> Department of Pathology, Section of Neuropathology, Translational Neurodegeneration Research and Neuropathology Lab, University of Oslo and Oslo University Hospital, Sognsvannsveien 20, 0372 Oslo, Norway

<sup>2</sup> Pahnke Laboratory (Drug Development and Chemical Biology), Lübeck Institute of Experimental Dermatology (LIED), University of Lübeck and University Medical Center Schleswig-Holstein, Ratzeburger Allee 160, 23538 Lübeck, Germany

<sup>3</sup> Department of Pharmacology, Faculty of Medicine, University of Latvia, Jelgavas iela 3, 1004 Rīga, Latvia

<sup>4</sup> Department of Neurobiology, The George S. Wise Faculty of Life Sciences, Tel Aviv University, Tel Aviv 6997801, Israel

\* Correspondence: jens.pahnke@gmail.com; Tel.: +47-23071466

† These authors contributed equally to this work.

**Abstract:** Alzheimer's disease (AD) is the most common cause of dementia. Fingolimod has previously shown beneficial effects in different animal models of AD. However, it has shown contradictory effects when it has been applied at early disease stages. Our objective was to evaluate fingolimod in two different treatment paradigms. To address this aim, we treated male and female APP-transgenic mice for 50 days, starting either before plaque deposition at 50 days of age (early) or at 125 days of age (late). To evaluate the effects, we investigated the neuroinflammatory and glial markers, the A $\beta$  load, and the concentration of the brain-derived neurotrophic factor (BDNF). We found a reduced A $\beta$  load only in male animals in the late treatment paradigm. These animals also showed reduced microglia activation and reduced IL-1 $\beta$ . No other treatment group showed any difference in comparison to the controls. On the other hand, we detected a linear correlation between BDNF and the brain A $\beta$  concentrations. The fingolimod treatment has shown beneficial effects in AD models, but the outcome depends on the neuroinflammatory state at the start of the treatment. Thus, according to our data, a fingolimod treatment would be effective after the onset of the first AD symptoms, mainly affecting the neuroinflammatory reaction to the ongoing A $\beta$  deposition.

**Keywords:** FTY720; fingolimod; Gilenya; APPPS1; Alzheimer's disease; amyloid beta; treatment



**Citation:** Bascuñana, P.; Brackhan, M.; Möhle, L.; Wu, J.; Brüning, T.; Eiriz, I.; Jansone, B.; Pahnke, J. Time- and Sex-Dependent Effects of Fingolimod Treatment in a Mouse Model of Alzheimer's Disease.

*Biomolecules* **2023**, *13*, 331. <https://doi.org/10.3390/biom13020331>

Academic Editor: Xiaobo Mao

Received: 15 December 2022

Revised: 14 January 2023

Accepted: 7 February 2023

Published: 9 February 2023



**Copyright:** © 2023 by the authors. Licensee MDPI, Basel, Switzerland. This article is an open access article distributed under the terms and conditions of the Creative Commons Attribution (CC BY) license (<https://creativecommons.org/licenses/by/4.0/>).

## 1. Introduction

Alzheimer's disease (AD) is the most common cause of dementia and affects over 30 million people worldwide [1]. AD is characterized by the accumulation of different neurotoxic proteins, e.g., amyloid- $\beta$  (A $\beta$ ) in plaques and tau as neurofibrillary tangles, leading to neurodegeneration, neuronal loss, and irreversible cognitive decline [2,3]. The causes responsible for the accumulation of A $\beta$  and tau in the brain remain unclear. Even though no successful therapeutic strategies have been developed, several molecular mechanisms involved in the pathogenesis of AD have been suggested: A $\beta$  overproduction and impaired A $\beta$  clearance, dysregulated tau phosphorylation, altered glutamatergic neurotransmission, as well as astrocyte and microglia activation prior to the clinical onset [4–6]. All of these proposed mechanisms can be used to identify new treatment targets for AD as mono- or multi-targeted therapies.

### *Fingolimod*

Fingolimod (FTY720, Gilenya; Novartis, Basel, Switzerland), a substrate of sphingosine kinases, targets several of the mechanisms mentioned above. The compound binds to

sphingosine-1-phosphate (S1P) receptors in its phosphorylated state [7]. The main pharmacologic effect of fingolimod is immunomodulation by lymphocyte sequestration in the lymph nodes by inhibiting the function of S1P<sub>1</sub> receptors in lymphocyte egression [8,9]. It was first clinically tested to modulate allograft rejection after a kidney transplantation [10]. However, the S1P<sub>1</sub> receptor is also involved in diverse functions in the central nervous system (CNS), such as neurogenesis, astrocyte activation and proliferation, and the communication between astrocytes, neurons, and the blood–brain barrier (BBB) [11]. Furthermore, fingolimod regulates the biosynthesis of sphingolipids, which play important roles in neurodegenerative diseases [12]. For these reasons, fingolimod has been tested in different animal models of neurodegenerative and neuroinflammatory diseases (reviewed in [13]). In addition, fingolimod has shown promising inhibitory effects on A $\beta$  toxicity and synthesis *in vitro*. Fingolimod ameliorated A $\beta$  neurotoxicity in neuronal cultures, reducing the neuronal death probably by increasing the brain-derived neurotrophic factor (BDNF) concentration [14,15]. The multiple pathways targeted by fingolimod suggest that this drug may be a promising therapy for AD.

Fingolimod has been tested previously in animal models of AD. Various authors have reported on the beneficial effects of fingolimod treatments in mouse models of AD. More specifically, it decreased the A $\beta$  production and/or deposition, induced neuroprotection, reduced neuroinflammation, reduced the occurrence of psychosis-like behaviour, and improved the cognitive function [16–25].

However, Takasugi and colleagues reported contradictory effects in an APP transgenic model (A7 model, human APP695 harbouring Swedish (K670N, M671L) and Austrian (T714I) mutations under control of Thy1.2 promoter of unknown genetic background [26]), showing a decrease in A $\beta$ 40, but an increase in A $\beta$ 42 [16]. This study is the only treatment that started before the manifestation of the first plaques, and therefore, also before onset of neuroinflammation.

In addition, fingolimod has been shown to reverse most of the A $\beta$ -induced changes in the gene expression of 12-month-old APP transgenic mice with London (V642I) mutation (FVB-Tg[Thy1; APP695/Ld2] [27]), but it had no beneficial effect on the 3-month-old APP transgenic mice [28]. Thus, the adequate timing of fingolimod treatments still needs to be elucidated.

Here, we aim to evaluate the effect of commencing a fingolimod treatment at two relevant time points: (i) before or at the very early stages of plaque deposition and (ii) at advanced stages of plaque deposition when neuroinflammatory activation was already present in our animal model of AD.

## 2. Results

To evaluate the impact of the starting point on the efficacy of fingolimod treatment in AD, we investigated alterations in weight, behaviour, A $\beta$  load, neuroinflammatory reaction, and BDNF in a mouse model of AD at two different ages.

### 2.1. Weight Development during Fingolimod Treatment

The fingolimod treatment in the drinking water did not affect the water consumption (data not shown) or body weight evolution of the animals at any of the ages tested (Figure 1). No significant differences were found.

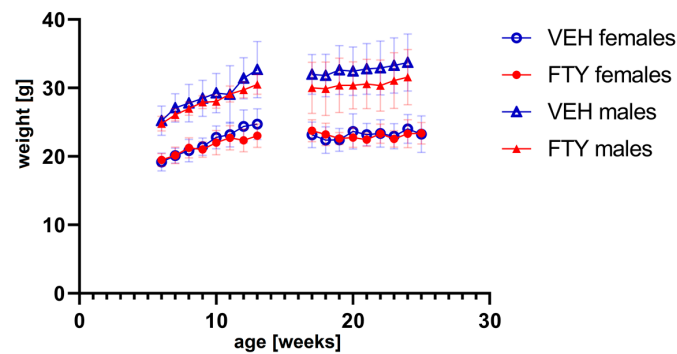


**Figure 1.** The graph shows the weight progression of early treated (left) and late treated animals (right) for all experimental groups. FTY—fingolimod (FTY720)-treated animals; VEH—vehicle-treated control animals. Data are presented as mean  $\pm$  SD;  $n = 8$  in all groups, except for the late treatment males ( $n = 13$ ). Statistical analysis was performed using two-way ANOVA (mixed-effects model). No significant differences were found.

### 2.2. Effects of Fingolimod on Activity or Spatial Orientation

The fingolimod treatment had no alternating effects on the overall daily activity of the mice neither in the light nor at the dark phase (Appendix A—Figure A1). The spatial orientation performance testing did not reveal significant differences (Appendix A—Figure A2).

### 2.3. Effects of Fingolimod on A $\beta$ Load

When the treatment was started at 125 days of age (late treatment), fingolimod reduced the deposition of insoluble A $\beta$  ( $9.1 \pm 2.6$  vs.  $12.9 \pm 3.6$  ng/mg brain,  $p = 0.003$ ) and the accumulation of soluble A $\beta$  ( $5.5 \pm 2.6$  vs.  $7.9 \pm 3.9$  pg/mg brain,  $p = 0.006$ ) in males. However, no differences were found in the female animals when we measured only insoluble A $\beta$  load ( $14.8 \pm 2.2$  vs.  $14.1 \pm 1.2$  pg/mg brain,  $p = 0.47$ ) (Figure 2).

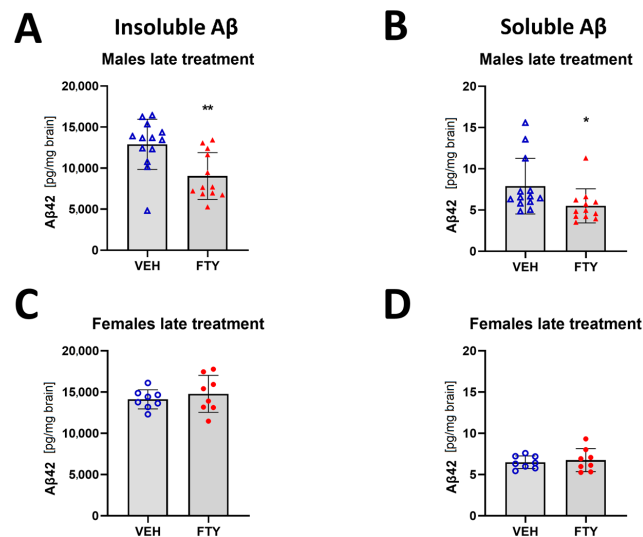


**Figure 2.** Quantification of insoluble (A,C) and soluble (B,D) A $\beta$ 42 for late treated males (A,B) and females (C,D) APPtg mice. Data are presented as mean  $\pm$  SD;  $n = 8$  (except for males VEH,  $n = 13$ ; FTY,  $n = 12$ ). Significance was calculated using Wilcoxon–Mann–Whitney test, and it is given as \*:  $p \leq 0.05$ , \*\*:  $p \leq 0.01$ .

In addition, the early treated female and male mice did not show differences in insoluble A $\beta$  compared to their respective control groups (starting treatment at 50 days of age;  $5.6 \pm 0.9$  and  $4.9 \pm 0.7$  pg/mg brain vs.  $5.1 \pm 0.9$  and  $4.9 \pm 0.8$  pg/mg brain, respectively) (Figure 3).

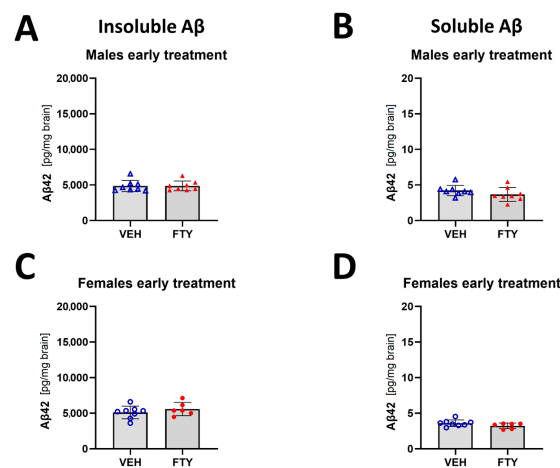


**Figure 3.** Quantification of insoluble (A,C) and soluble (B,D) A $\beta$ 42 for early treated males (A,B) and females (C,D). Data are presented as mean  $\pm$  SD;  $n = 8$  (except for FTY treatment females,  $n = 6$ ). Significance was calculated using Wilcoxon–Mann–Whitney test.

#### 2.4. Effects of Fingolimod on the Reaction of Microglia and Astrocytes

Assessment of microglia immunostaining against Iba1 revealed a decrease in the microglia coverage (total area covered by microglia;  $7.12 \pm 0.01\%$  vs.  $9.26 \pm 0.01\%$ ;  $p = 0.004$ ) and microglia density (number of cells per  $10 \text{ mm}^2$  area;  $2175 \pm 350$  vs.  $2832 \pm 395$  cells/ $10 \text{ mm}^2$ ;  $p = 0.004$ ; Figure 4A–D) in the late FTY-treated males compared to their VEH-treated controls. However, the fingolimod treatment had no effect on microglial activation in the female animals, which is similar to the unchanged A $\beta$  levels.

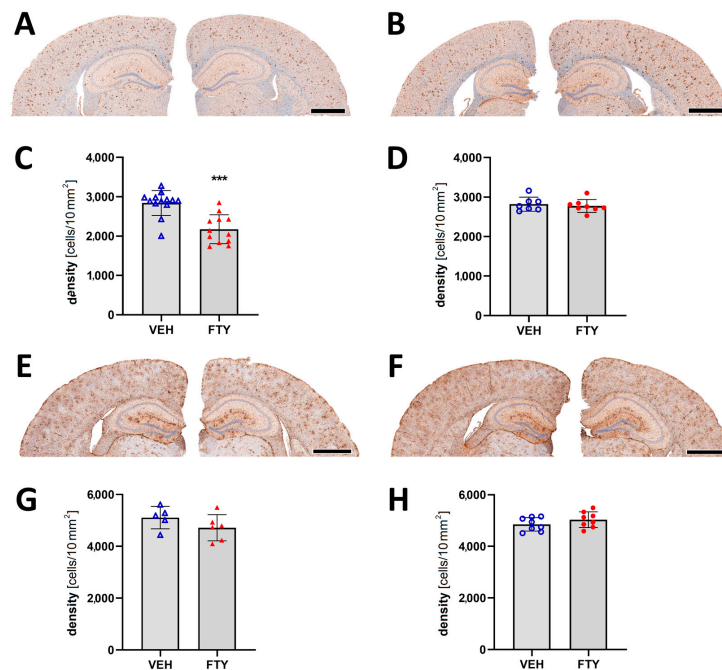


**Figure 4.** Evaluation of micro- and astrogliosis in mice with late treatment paradigm (at 175 days of age). (A,B) Representative images of Iba1 immunostaining of male (A) and female (B) mice. Microglia activation was determined as density of IBA1-positive cells in males (C) and females (D). (E,F) Representative images of GFAP immunostaining in males (E) and females (F). Astrocyte density in males (G) and females (H). Data are presented as mean  $\pm$  SD; VEH males  $n = 13$  for IBA1,  $n = 5$  for GFAP, FTY males  $n = 12$  for IBA1,  $n = 6$  for GFAP, females  $n = 8$ . Significance was calculated using Student's *t*-test, and it is given as \*\*\*:  $p \leq 0.001$ . Scale bars: 1 mm.

Astrocyte activation was measured as the astrocyte density in the cortex, and it was not significantly altered by the fingolimod treatment for any of the groups (Figure 4E–H).

### 2.5. Effects of Fingolimod on Brain Cytokine Levels

Microglial cells are important immune cells in the brain, and they are the cells that appear to be activated in the brain tissue when A $\beta$  deposition starts. Therefore, we wanted to characterize the effect of fingolimod on the cytokine profile in the brain. Here, we found that the pro-inflammatory cytokine IL-1 $\beta$  level was reduced in the late treated males ( $2.34 \pm 0.48$  vs.  $3.19 \pm 0.76$  pg/100 mg brain,  $p = 0.004$ ) (Figure 5). No differences were observed in the other cytokines that were measured (IFN-g, IL-2, IL-4, IL-6, IL-10, MCP-1, and TNF- $\alpha$ ) or in other experimental groups (females and younger animals).

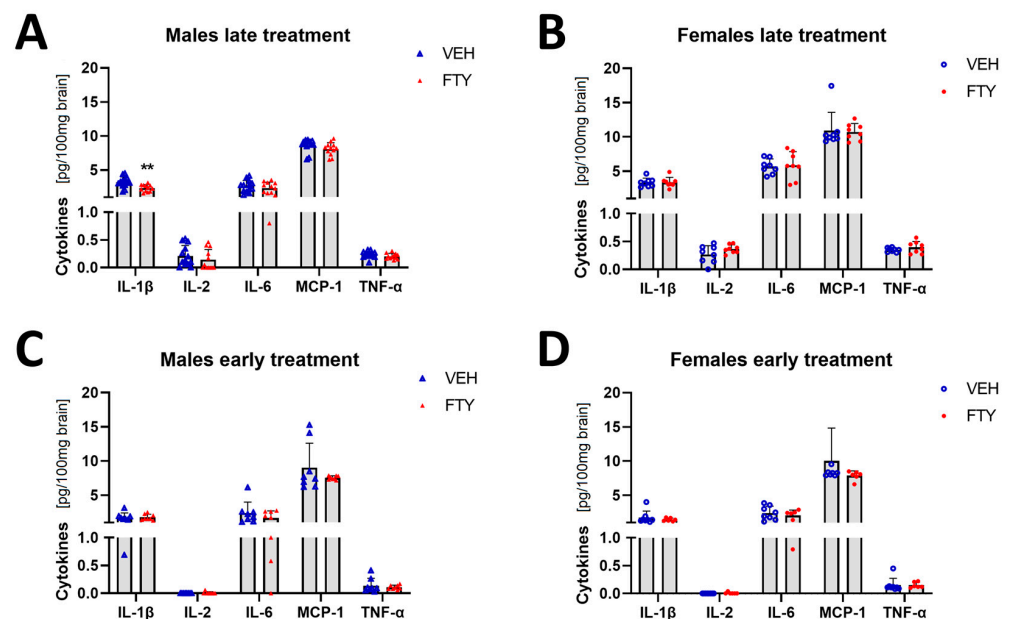


**Figure 5.** Levels of selected cytokines in brain tissue in late and early treated animals. (A,B) Quantification of IL-1 $\beta$ , IL-1, IL-6, MCP-1, and TNF $\alpha$  in late treated males (A) and females (B). (C,D) Quantification of the cytokines in early treated males (C) and females (D). Data are presented as mean  $\pm$  SD;  $n = 8$  except late treatment males (VEH  $n = 13$ ; FTY  $n = 12$ ) and early FTY treatment females ( $n = 6$ ). Significance was calculated using Student's  $t$ -test, and it is given as \*\*:  $p \leq 0.01$ .

### 2.6. Effects of Fingolimod on Cerebral BDNF Levels

Previous studies have reported that fingolimod increased the BDNF concentration in the brain [20,29]. Thus, we quantified BDNF in the brain extracts in all of the experimental groups. We found a trend (non-significant) of decreased BDNF levels only in late treated males in comparison to that of their control group ( $70.1 \pm 17.2$  vs.  $84.3 \pm 19.3$ ,  $p = 0.06$ ). The remaining groups showed no significant difference in the BDNF levels (Figure 6). However, the BDNF concentration positively correlated to the A $\beta$  levels in all of the groups ( $r = 0.785$ ;  $p < 0.001$ ).

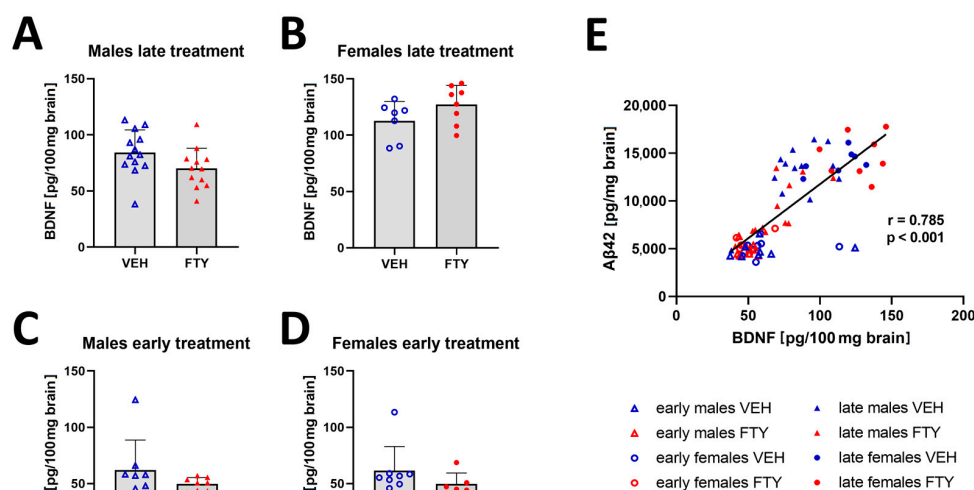


**Figure 6.** Amount of BDNF in brain tissues. (A–D) Graphs show the quantification of BDNF in brain tissues of late treated male (A) and female (B) and early treated male (C) and female (D) APPtg mice. (E) Linear regression analysis between brain BDNF and Aβ concentrations show a positive correlation between both of the proteins. Data are presented as mean ± SD;  $n = 8$ , except for late treated males VEH,  $n = 13$ ; FTY,  $n = 12$  and early treated females ( $n = 6$ ). Significance between experimental groups was calculated using the Wilcoxon–Mann–Whitney test. Correlation coefficient was analysed using Pearson’s correlation test.

### 3. Discussion

The present study shows that fingolimod has reducing effects on the Aβ load in our animal model of AD *only* when it is administered at a later stage of the disease. Fingolimod was reported previously to have beneficial effects on the animal models of AD [16–23,25]. However, two studies showed no effect of this treatment when it was administered at the early stages in contrast to the older animals [28,30], which is similar to our finding. Furthermore, the beneficial effect of our treatment was only apparent in male mice, while female mice showed no effect in any of the tested treatment paradigms. This sex-selective effect was not observed previously in any of the studies published, except for a study on patients, in which women were reported to have higher occurrence of adverse effects, mainly infections [31]. It is common that the treatment effects are different between male and female individuals. Interestingly, a recent review by the Norwegian Health Institute (FHI: Folkehelseinstituttet) of patient studies that were exclusively performed in Norway between 2017 and 2022 found that there is a substantial lack of systematically analysing the sex-related effects: 133 studies reported sex-related analyses and 178 did not [32]. Metabolically, male and female individuals are different also at different ages [33,34], and thus, the treatment response differences should be assumed as normal. In older age, increasing differences in anabolic hormone production and degradation adds to the apparent biochemical sex differences [35]. Not only biochemical differences, but also differences in the function of the immune system and its response towards Aβ, esp. microglia, could be influenced by sex (reviewed in [36]).

Fingolimod’s main pharmacologic effect is immunomodulation by lymphocyte sequestration, thus reducing the numbers of T and B cells in circulation [8]. It has been shown that effect of fingolimod depends on the inflammatory status of the animals [37]. Therefore, we hypothesized that in order to observe a positive treatment effect, the microglia must be activated before starting the treatment. We proposed to evaluate the effect of the immunomodulatory treatment with fingolimod in two groups of APPtg mice: those that were early on in the disease at 50–100 days (i.e., before extensive microglial activation) and those that were late in its progression at 125–175 days (when microglia are highly

activated) [38]. Our study confirms that the fingolimod treatment is only effective in reducing both microglia activation and plaque load when it is administered at the late phase of A $\beta$  deposition. Although S1P receptors are involved in different mechanisms in astrocytes [39–42], we did not find any alterations in the astrocyte activation of the APPtg mice with the fingolimod treatment.

As fingolimod's main effect is immunomodulation, we also evaluated its effect on the brain cytokine levels in the APPtg mice. We found that the fingolimod treatment reduced the pro-inflammatory cytokine IL-1 $\beta$  level. The reduction of inflammatory markers has been described previously in other studies with AD models, but also, with other neurodegeneration models. This reduction might be related to the decrease in the activated microglia in the late-treated males, as observed in our study. On the other hand, several studies have found an increase in BDNF after the fingolimod treatment [14,20,29,43–47]. Contrarily, we found even a non-significant trend of decreased BDNF concentration in male mice treated with fingolimod in comparison to that of their vehicle-treated control group. Nevertheless, we observed a direct correlation between BDNF and A $\beta$  levels in all of the groups. This increase in BDNF in APP<sup>+</sup>/PS1<sup>+</sup> mice (Prp-APP<sup>swe</sup>/Prp-PS1 $\Delta$ E9 [48]) has previously been reported [49]. Thus, the decrease observed in the males of the treated group might be sole due to the reduction in the A $\beta$  load in these animals, and not because of a direct effect of the fingolimod treatment on the BDNF concentration.

In summary, we have shown that the fingolimod treatment has beneficial effects on an AD model, but its success depends on the neuroinflammatory state at the beginning of the treatment and the subject's sex. Thus, according to our data and as previously described in [23], fingolimod treatments would be more effective after the onset of the first AD symptoms, mainly affecting the neuroinflammatory reaction towards A $\beta$  deposits.

## 4. Material and Methods

### 4.1. Animal Models and Breeding Schemes

Heterozygous APP transgenic (APPtg) mice (APPPS1–21 [50]) were used in this study. APPPS1-21 mice have a combined APP (Swedish mutations) and PS1 (L166P mutation) transgene under control of the Thy1-promoter, leading primarily to pathological A $\beta$  production in the frontocortical neurons and the first cortical A $\beta$  plaques at 45–50 days of age, which occurs much later also in other brain regions, but to a significant lesser extend (e.g., hippocampus).

The transgenic breeding programs were maintained with male heterozygous, transgene-positive breeders and C57BL/6J transgene-negative females. The animals were housed in the animal care facility of the Department of Comparative Medicine at the Oslo University Hospital (Norway) with a 12 h/12 h light/dark cycle at a temperature of 22 °C with free access to irradiated food and autoclaved, acidified water. All of the experiments were approved by the competent authorities and conducted according to the European Union Directive and regional laws.

### 4.2. Experimental Design—Treatment Paradigms

Animals were distributed into eight experimental groups (see also Table A1):

- (a) Early vehicle-treated males;
- (b) Early FTY-treated males;
- (c) Early vehicle-treated females;
- (d) Early FTY-treated females;
- (e) Late vehicle-treated males;
- (f) Late FTY-treated males;
- (g) Late vehicle-treated females;
- (h) Late FTY-treated females.

Fingolimod (FTY720, Sigma-Aldrich, Darmstadt, Germany) was given dissolved in drinking water at a dose of 1 mg/kg bodyweight per day. The animals had a mean uptake between 2.8 mL (late treated males) and 3.5 mL (early treated males) per day from the drinking water. The FTY720 dose in water was corrected according to water consumption

in each group. The treatment was administered for 50 days starting at 50 or 125 days of age, respectively, depending on the experimental group (Figure 7). The body weight and water consumption rate of the animals was controlled weekly to monitor potential side effects and to adjust the dose.

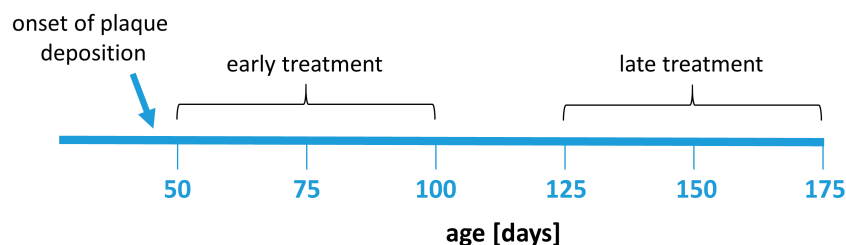


**Figure 7.** Experimental design. Animals were treated with fingolimod in two treatment paradigms: early treatment (between 50 and 100 days of age) or late treatment (between 125 and 175 days of age). The treatment duration (50 days) was the same in all treatment groups.

### 4.3. Assessment of Activity and Cognitive Performance

#### 4.3.1. Assessment of Activity

The activity of the mice was recorded with infrared sensor-based technology (TSE Systems GmbH, Berlin, Germany) for a period of 48 h (plus 24 h for acclimatisation). Within this period, the mice were housed individually in small standard cages and a typical habitat. The treatment of the mice was performed daily between 9 a.m. and 10 a.m., which was excluded from the activity analysis. The movement of the mice was detected by infrared sensors located on top of the cages. The movements were integrated over 10 min time intervals. Subsequently, the data were analysed using the Phenomaster Software (TSE Systems GmbH, Berlin, Germany) and displayed cumulatively as a function of time (Figure A1).

#### 4.3.2. Assessment of Spatial Orientation Performance

A modified version of our previously published protocol was applied [51–54]. Briefly, the mice were trained for six days, with four consecutive trials per day and a short recovery period of 60 s between the trials. On day 7, the mice were subjected to a probe trial, where the hidden platform was removed, and visual cue trials, where the platform was clearly marked with a visual cue to detect severe visual impairments. Data were acquired using EthoVision XT (version 15, Noldus Information Technology BV, Wageningen, The Netherlands). The animals were treated by gavage after behavioural testing each day to avoid interference due to potential acute effects.

### 4.4. Tissue Collection and Processing

The mice were sacrificed by ketamine/xylazine overdose (400 mg/kg ketamine, 40 mg/kg xylazine) and transcardially perfused with ice-cold 0.1 M phosphate-buffered saline (PBS). The brains were removed, and the cerebrums were divided into two hemispheres. One hemisphere was kept in 4% paraformaldehyde (PFA) in 0.1 M PBS for immunohistochemical processing. The other hemisphere was snap frozen in liquid nitrogen and stored in  $-80^{\circ}\text{C}$  until further protein extraction.

### 4.5. Immunohistochemistry Labelling and Morphological Quantification

Formalin-fixed hemispheres were embedded in paraffin and sliced into four-micrometer-thick coronal sections using a rotation microtome (HM355S, Leica Biosystems GmbH, Nussloch, Germany), as described previously [38,51–53,55–61]. The sections (bregma  $-2.0$  mm) were stained for microglia (anti-IBA1, 1:1000, FUJIFILM Wako Chemicals Europe GmbH, 019–19741) or astrocytes (anti-GFAP, 1:500, Agilent, USA, Z033401-2) using a BOND-III<sup>®</sup> automated immunostaining system (Leica Biosystems GmbH, Nussloch, Germany) with a haematoxylin counterstain (provided with the staining kit, Bond Polymer Refine Detection,

DS9800). The sections for anti-IBA1 staining were pre-treated with citric acid for 20 min before staining. For anti-GFAP staining, the Bond Enzyme Pre-Treatment Kit (AR9551, Leica Biosystems GmbH, Nussloch, Germany) was applied to the sections for 10 min.

After staining, the tissue sections were digitized at 230 nm resolution using a Panoramic MIDI II slide scanner (3DHISTECH Ltd., Budapest, Hungary).

A quantitative analysis of the microglia and astrocytes in the cortex of each animal was performed automatically as previously described by us [38,55,56,61] using deep-learning algorithms generated with the DeePathology™ STUDIO (DeePathology Ltd., Ra'anana, Israel). We generated specific algorithms to identify IBA1+ cells or GFAP+ cells. The algorithms were applied for the ROIs (Figure 8A). The cell density (number per ROI) and relative areal coverage (% cell area per total ROI) were calculated for each animal.

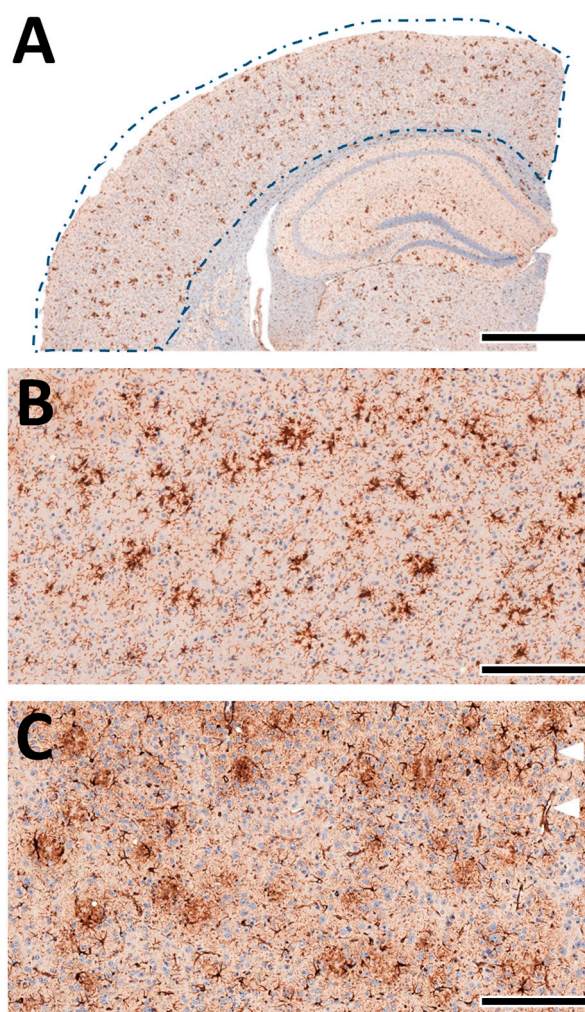


**Figure 8.** Machine learning-assisted morphological analyses of cortex pathology. (A) Schematic presentation of the analysed cortex region (from Figure 4A, left). The brain tissue was automatically detected within the manually marked ROI. (B) Staining of IBA1+ cells in the cortex. The microglia nicely accumulate near-insoluble A $\beta$  deposits and delineate amyloid plaques. (C) Staining of GFAP+ cells in the cortex. Astrocytes show a more diffuse pattern with localised perivascular pronunciation (white triangles). Scale bars: (A) 1 mm, (B,C) 50  $\mu$ m.

#### 4.6. Quantification of A $\beta$

We performed the quantification of the brain A $\beta$  levels using an electrochemiluminescence immunoassay. Thus, we homogenized the brain hemispheres and soluble and insoluble A $\beta$  fractions were extracted in TBS and guanidine buffer, respectively [51]. Im-

immunoassays were performed using the V-PLEX Plus A $\beta$ 42 Peptide (4G8) Kit and an MESO QuickPlex SQ120 machine according to the manufacturer's instructions (K150SLG, Meso Scale Diagnostics LLC, Rockville, MD, USA). The results were normalized to the sample weight. The brain A $\beta$ 42 content was calculated as pg/mg brain.

#### 4.7. Quantification of BDNF and Cytokines

We performed a quantification of the BDNF and inflammatory cytokine levels in the brain by immunoassay. To achieve this aim, brain homogenates were extracted using lysis buffer (Phosphate buffer saline + 1% Triton X-100 + phosphatase inhibitor + protease inhibitor) at 2  $\mu$ L/mg brain homogenate. The samples were homogenized for 30 s (SpeedMill PLUS, Analytik Jena GmbH, Jena, Germany) and centrifuged at 16,000 g for 15 min at 4 °C. Supernatants were diluted 4-fold using a working solution (Meso Scale Diagnostics LLC, Rockville, MD, USA), and immunoassays were performed using the U-PLEX Kit for BDNF and cytokines (IL-2, IL-4, IL-6; TNF $\alpha$ , IFN $\gamma$ ) and a MESO QuickPlex SQ120 machine following the manufacturer's instructions.

#### 4.8. Statistical Analyses

All of the statistical analyses were performed using GraphPad Prism 9 software (GraphPad Software, CA, USA). We verified the data for Gaussian normal distribution by using the Shapiro–Wilk normality test. The Student's *t*-test or Mann–Whitney test were performed to determine the significant differences between the two groups. The correlation coefficient was analysed using Pearson's correlation test. Data are presented as means  $\pm$  standard deviation (SD). Differences were considered to be statistically significant when  $p < 0.05$ . The number of subjects (*n*) is reported in the figure legends and is summarized in Appendix B (Table A1). Detailed statistical methods are summarized in Appendix B (Table A2).

**Author Contributions:** Conceptualization, P.B. and J.P.; Methodology, P.B., M.B., L.M., J.W., T.B., I.E. and J.P.; Validation, P.B.; Formal Analysis, P.B. and M.B.; Investigation, P.B. and M.B.; Data Curation, P.B. and M.B.; Writing—Original Draft Preparation, P.B., M.B. and J.P.; Writing—Review and Editing, P.B., M.B., L.M., J.W., T.B., I.E., B.J. and J.P.; Visualization, P.B. and J.P.; Supervision, J.P.; Project Administration, P.B. and J.P.; Funding Acquisition, B.J. and J.P. All authors have read and agreed to the published version of the manuscript.

**Funding:** J.P. received funding from the German Research Foundation (DFG, Germany; #263024513), HelseSØ (Norway; #2019054, #2019055, and #2022046), Barnekreftforeningen (Norway; #19008), EEA and Norway grants Kappa programme [Iceland, Liechtenstein, Norway, Czech Republic; #TO01000078 (TAČR TARIMAD)], Norges forskningsråd [NFR, Norway; #295910 (NAPI), #327571 (PETABC)]. PETABC is an EU Joint programme—Neurodegenerative Disease Research (JPND) project. PETABC is supported through the following funding organizations under the aegis of JPND—[www.jpnd.eu](http://www.jpnd.eu): NFR (Norway; #327571), FFG (Austria; #882717), BMBF (Germany; #01ED2106); MSMT (Czech Republic; #8F21002), Latvia; #ES RTD/2020/26, ANR (France; #20-JPW2-0002-04), SRC (Sweden; #2020-02905). L.M. appreciated the support by Nasjonalforeningen (Norway; #16154). B.J. appreciated the support by Latvia #ES RTD/2020/26 (PETABC).

**Institutional Review Board Statement:** The animal study protocol was approved by the local authorities (FOTS 7771, 24 January 2015; FOTS 20540, 14 October 2019; IV2-2022 1 December 2022) for studies involving animals.

**Informed Consent Statement:** Not applicable.

**Data Availability Statement:** Data files and figures can be downloaded from the ABCS1P project at <http://www.doi.org/10.17605/OSF.IO/VWQ58> (accessed on 1 February 2023).

**Conflicts of Interest:** The authors declare no conflict of interest.

## Abbreviations

AD, Alzheimer's disease; FTY720, fingolimod; GFAP, glial fibrillary acid protein; IBA1, ionized calcium-binding adaptor protein-1; PBS, phosphate-buffered saline; PCR, polymerase chain reaction; PFA, paraformaldehyde; ROI, region of interest; SD, standard deviation; SDS-PAGE, sodium dodecyl sulfate polyacrylamide gel electrophoresis.

## Appendix A. Activity and Cognitive Performance Assessment

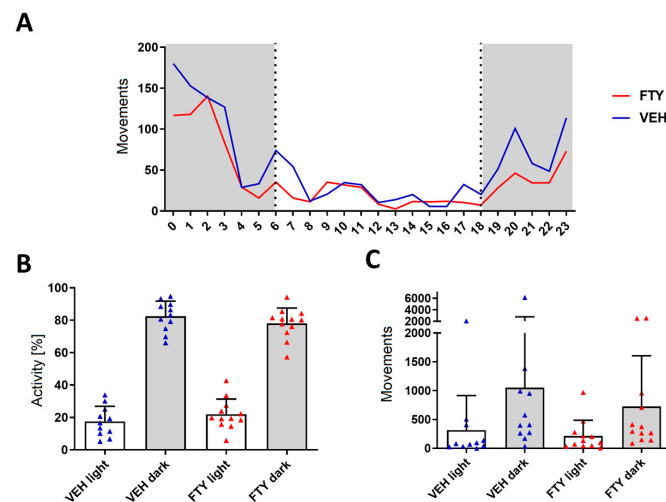


**Figure A1.** Assessment of the circadian activity during a 24 h period revealed no differences between VEH-treated (blue triangles) and FTY-treated (red triangles) males. Animals were treated according to the early treatment paradigm. (A) Mean hourly count of movements of animal groups (grey indicates dark hours; white indicates light hours of the day). (B) Relative distribution of the activity and (C) number of detected movements for each experimental group during light and dark hours. Significance in activity between treatment groups was calculated using the Student's *t*-test. Data are presented as mean  $\pm$  SD, VEH  $n = 11$ , FTY  $n = 12$ .

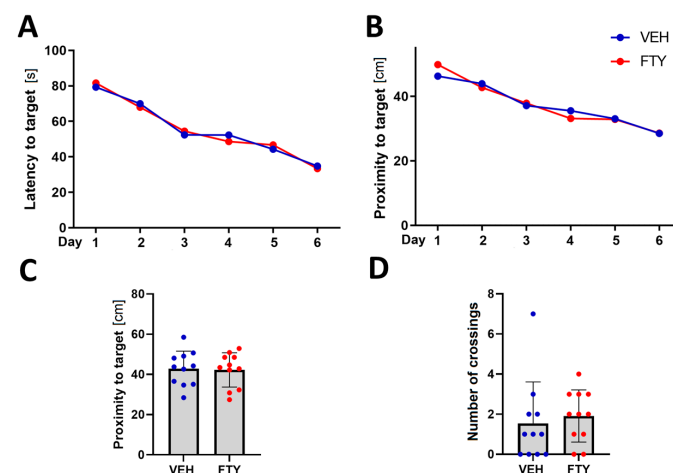


**Figure A2.** Spatial orientation testing using water maze revealed no significant differences between VEH-treated (blue circles) and FTY-treated (red circles) females. Animals were treated according to the early treatment paradigm. (A) Time latency [s] average of each experimental group to find the platform during training trials. (B) Proximity average [cm] during training. (C) Proximity to target and (D) number of target crossings ( $n \in N$ ) during the probe trial. Significance between treatment groups was calculated using the Student's *t*-test (C) or Wilcoxon–Mann–Whitney test (D). Data are presented as mean (A,B) and mean  $\pm$  SD (C,D), VEH  $n = 11$ , and FTY  $n = 11$ .

## Appendix B. Statistics

**Table A1.** Summary of experimental groups.

Paradigm	Experimental Group	Number of Animals
early (50–100 d)	VEH treatment males	8, (11) <sup>1</sup>
	FTY treatment males	8, (11) <sup>1</sup>
	VEH treatment females	8, (11) <sup>1</sup>
	FTY treatment females	6 (of 8) <sup>2</sup> , (11) <sup>1</sup>
late (125–175 d)	VEH treatment males	13
	FTY treatment males	12 (of 13) <sup>2</sup>
	VEH treatment females	8
	FTY treatment females	8

<sup>1</sup> Numbers in parentheses correspond to animal used for spatial orientation assessment only. This extra group was treated with FTY or VEH using oral gavage. <sup>2</sup> Some animals died during the experiment.

**Table A2.** Statistical tests used for the evaluation of differences between experimental groups for each variable studied.

Variable	Statistical Test
animal weight	two-way ANOVA (mixed effects)
A $\beta$ concentration	Wilcoxon–Mann–Whitney test
microglia density	Student's <i>t</i> -test
astrocyte density	Student's <i>t</i> -test
cytokine concentration	Student's <i>t</i> -test
BDNF concentration	Wilcoxon–Mann–Whitney test
activity	Student's <i>t</i> -test
spatial orientation (proximity and number of crossing)	Student's <i>t</i> -test and Wilcoxon–Mann–Whitney test

## References

- Alzheimer Association Report. 2020 Alzheimer's disease facts and figures. *J. Alzheimers Dement.* **2020**, *16*, 391–460. [\[CrossRef\]](#)
- Thinakaran, G.; Koo, E.H. Amyloid precursor protein trafficking, processing, and function. *J. Biol. Chem.* **2008**, *283*, 29615–29619. [\[CrossRef\]](#)
- Scheltens, P.; De Strooper, B.; Kivipelto, M.; Holstege, H.; Chetelat, G.; Teunissen, C.E.; Cummings, J.; van der Flier, W.M. Alzheimer's disease. *Lancet* **2021**, *397*, 1577–1590. [\[CrossRef\]](#)
- Pahnke, J.; Langer, O.; Krohn, M. Alzheimer's and ABC transporters—new opportunities for diagnostics and treatment. *Neurobiol. Dis.* **2014**, *72 Pt A*, 54–60. [\[CrossRef\]](#)
- Pahnke, J.; Walker, L.C.; Scheffler, K.; Krohn, M. Alzheimer's disease and blood-brain barrier function—Why have anti-beta-amyloid therapies failed to prevent dementia progression? *Neurosci. Biobehav. Rev.* **2009**, *33*, 1099–1108. [\[CrossRef\]](#)
- Lane, C.A.; Hardy, J.; Schott, J.M. Alzheimer's disease. *Eur. J. Neurol.* **2018**, *25*, 59–70. [\[CrossRef\]](#)
- Mandala, S.; Hajdu, R.; Bergstrom, J.; Quackenbush, E.; Xie, J.; Milligan, J.; Thornton, R.; Shei, G.J.; Card, D.; Keohane, C.; et al. Alteration of lymphocyte trafficking by sphingosine-1-phosphate receptor agonists. *Science* **2002**, *296*, 346–349. [\[CrossRef\]](#)
- Chiba, K.; Yanagawa, Y.; Masubuchi, Y.; Kataoka, H.; Kawaguchi, T.; Ohtsuki, M.; Hoshino, Y. FTY720, a novel immunosuppressant, induces sequestration of circulating mature lymphocytes by acceleration of lymphocyte homing in rats. I. FTY720 selectively decreases the number of circulating mature lymphocytes by acceleration of lymphocyte homing. *J. Immunol.* **1998**, *160*, 5037–5044. [\[CrossRef\]](#)
- Pham, T.H.; Okada, T.; Matloubian, M.; Lo, C.G.; Cyster, J.G. S1P1 receptor signaling overrides retention mediated by G alpha i-coupled receptors to promote T cell egress. *Immunity* **2008**, *28*, 122–133. [\[CrossRef\]](#)
- Budde, K.; Schutz, M.; Glander, P.; Peters, H.; Waiser, J.; Liefeldt, L.; Neumayer, H.H.; Bohler, T. FTY720 (fingolimod) in renal transplantation. *Clin. Transpl.* **2006**, *20* (Suppl. S17), 17–24. [\[CrossRef\]](#)
- Brinkmann, V. Sphingosine 1-phosphate receptors in health and disease: Mechanistic insights from gene deletion studies and reverse pharmacology. *Pharmacol. Ther.* **2007**, *115*, 84–105. [\[CrossRef\]](#)
- Czubowicz, K.; Jesko, H.; Wencel, P.; Lukiw, W.J.; Strosznajder, R.P. The Role of Ceramide and Sphingosine-1-Phosphate in Alzheimer's Disease and Other Neurodegenerative Disorders. *Mol. Neurobiol.* **2019**, *56*, 5436–5455. [\[CrossRef\]](#)
- Bascuñana, P.; Möhle, L.; Brackhan, M.; Pahnke, J. Fingolimod as a Treatment in Neurologic Disorders Beyond Multiple Sclerosis. *Drugs RD* **2020**, *20*, 197–207. [\[CrossRef\]](#)
- Doi, Y.; Takeuchi, H.; Horiuchi, H.; Hanyu, T.; Kawanokuchi, J.; Jin, S.; Parajuli, B.; Sonobe, Y.; Mizuno, T.; Suzumura, A. Fingolimod phosphate attenuates oligomeric amyloid beta-induced neurotoxicity via increased brain-derived neurotrophic factor expression in neurons. *PLoS ONE* **2013**, *8*, e61988. [\[CrossRef\]](#)

15. Ruiz, A.; Joshi, P.; Mastrangelo, R.; Francolini, M.; Verderio, C.; Matteoli, M. Testing Abeta toxicity on primary CNS cultures using drug-screening microfluidic chips. *Lab Chip* **2014**, *14*, 2860–2866. [[CrossRef](#)]
16. Takasugi, N.; Sasaki, T.; Ebinuma, I.; Osawa, S.; Isshiki, H.; Takeo, K.; Tomita, T.; Iwatsubo, T. FTY720/fingolimod, a sphingosine analogue, reduces amyloid beta/amyloid beta production in neurons. *PLoS ONE* **2013**, *8*, e64050. [[CrossRef](#)]
17. Asle-Rousta, M.; Kolahdooz, Z.; Dargahi, L.; Ahmadiani, A.; Nasoohi, S. Prominence of central sphingosine-1-phosphate receptor-1 in attenuating abeta-induced injury by fingolimod. *J. Mol. Neurosci.* **2014**, *54*, 698–703. [[CrossRef](#)] [[PubMed](#)]
18. Hemmati, F.; Dargahi, L.; Nasoohi, S.; Omidbakhsh, R.; Mohamed, Z.; Chik, Z.; Naidu, M.; Ahmadiani, A. Neurorestorative effect of FTY720 in a rat model of Alzheimer's disease: Comparison with memantine. *Behav. Brain Res.* **2013**, *252*, 415–421. [[CrossRef](#)]
19. Asle-Rousta, M.; Kolahdooz, Z.; Oryan, S.; Ahmadiani, A.; Dargahi, L. FTY720 (fingolimod) attenuates beta-amyloid peptide (A $\beta$ 42)-induced impairment of spatial learning and memory in rats. *J. Mol. Neurosci.* **2013**, *50*, 524–532. [[CrossRef](#)]
20. Fukumoto, K.; Mizoguchi, H.; Takeuchi, H.; Horiuchi, H.; Kawanokuchi, J.; Jin, S.; Mizuno, T.; Suzumura, A. Fingolimod increases brain-derived neurotrophic factor levels and ameliorates amyloid beta-induced memory impairment. *Behav. Brain Res.* **2014**, *268*, 88–93. [[CrossRef](#)]
21. Aytan, N.; Choi, J.K.; Carreras, I.; Brinkmann, V.; Kowall, N.W.; Jenkins, B.G.; Dedeoglu, A. Fingolimod modulates multiple neuroinflammatory markers in a mouse model of Alzheimer's disease. *Sci. Rep.* **2016**, *6*, 24939. [[CrossRef](#)]
22. Carreras, I.; Aytan, N.; Choi, J.K.; Tognoni, C.M.; Kowall, N.W.; Jenkins, B.G.; Dedeoglu, A. Dual dose-dependent effects of fingolimod in a mouse model of Alzheimer's disease. *Sci. Rep.* **2019**, *9*, 10972. [[CrossRef](#)]
23. Kartalou, G.-I.; Salgueiro-Pereira, A.R.; Endres, T.; Lesnikova, A.; Casarotto, P.; Pousinha, P.; Delanoë, K.; Edelmann, E.; Castrén, E.; Gottmann, K.; et al. Anti-Inflammatory Treatment with FTY720 Starting after Onset of Symptoms Reverses Synaptic Deficits in an AD Mouse Model. *Int. J. Mol. Sci.* **2020**, *21*, 8957. [[CrossRef](#)]
24. Krivinko, J.M.; Erickson, S.L.; MacDonald, M.L.; Garver, M.E.; Sweet, R.A. Fingolimod mitigates synaptic deficits and psychosis-like behavior in APP/PSEN1 mice. *Alzheimer's Dement. Transl. Res. Clin. Interv.* **2022**, *8*, e12324. [[CrossRef](#)]
25. Crivelli, S.M.; Luo, Q.; Kruijning, D.V.; Giovagnoni, C.; Mane-Damas, M.; den Hoedt, S.; Berkes, D.; De Vries, H.E.; Mulder, M.T.; Walter, J.; et al. FTY720 decreases ceramides levels in the brain and prevents memory impairments in a mouse model of familial Alzheimer's disease expressing APOE4. *Biomed Pharm.* **2022**, *152*, 113240. [[CrossRef](#)]
26. Yamada, K.; Yabuki, C.; Seubert, P.; Schenk, D.; Hori, Y.; Ohtsuki, S.; Terasaki, T.; Hashimoto, T.; Iwatsubo, T. Abeta immunotherapy: Intracerebral sequestration of Abeta by an anti-Abeta monoclonal antibody 266 with high affinity to soluble Abeta. *J. Neurosci.* **2009**, *29*, 11393–11398. [[CrossRef](#)]
27. Moechars, D.; Dewachter, I.; Lorent, K.; Reverse, D.; Baekelandt, V.; Naidu, A.; Tesseur, I.; Spittaels, K.; Haute, C.V.; Checler, F.; et al. Early phenotypic changes in transgenic mice that overexpress different mutants of amyloid precursor protein in brain. *J. Biol. Chem.* **1999**, *274*, 6483–6492. [[CrossRef](#)]
28. Jesko, H.; Wiczorek, I.; Wencel, P.L.; Gassowska-Dobrowolska, M.; Lukiw, W.J.; Strosznajder, R.P. Age-Related Transcriptional Deregulation of Genes Coding Synaptic Proteins in Alzheimer's Disease Murine Model: Potential Neuroprotective Effect of Fingolimod. *Front. Mol. Neurosci.* **2021**, *14*, 660104. [[CrossRef](#)] [[PubMed](#)]
29. Deogracias, R.; Yazdani, M.; Dekkers, M.P.J.; Guy, J.; Ionescu, M.C.S.; Vogt, K.E.; Barde, Y.-A. Fingolimod, a sphingosine-1 phosphate receptor modulator, increases BDNF levels and improves symptoms of a mouse model of Rett syndrome. *Proc. Natl. Acad. Sci. USA* **2012**, *109*, 14230–14235. [[CrossRef](#)]
30. Fagan, S.G.; Bechet, S.; Dev, K.K. Fingolimod Rescues Memory and Improves Pathological Hallmarks in the 3xTg-AD Model of Alzheimer's Disease. *Mol. Neurobiol.* **2022**, *59*, 1882–1895. [[CrossRef](#)]
31. Manni, A.; Direnzo, V.; Iaffaldano, A.; Di Lecce, V.; Tortorella, C.; Zoccolella, S.; Iaffaldano, P.; Trojano, M.; Paolicelli, D. Gender differences in safety issues during Fingolimod therapy: Evidence from a real-life Relapsing Multiple Sclerosis cohort. *Brain Behav.* **2017**, *7*, e00804. [[CrossRef](#)]
32. Østbø, N.M.; Vist, G.E.; Løchen, M.-L. Sex and Gender-based Analyses in Norwegian Treatment Studies: A Scoping Review. In *Folkehelseinstituttet*; Folkehelseinstituttet: Oslo, Norway, 2022; p. 44.
33. Costanzo, M.; Caterino, M.; Sotgiu, G.; Ruoppolo, M.; Franconi, F.; Campesi, I. Sex differences in the human metabolome. *Biol. Sex Differ.* **2022**, *13*, 30. [[CrossRef](#)]
34. Zhernakova, D.V.; Sinha, T.; Andreu-Sánchez, S.; Prins, J.R.; Kurilshikov, A.; Balder, J.-W.; Sanna, S.; Franke, L.; Kuivenhoven, J.A.; Zhernakova, A.; et al. Age-dependent sex differences in cardiometabolic risk factors. *Nat. Cardiovasc. Res.* **2022**, *1*, 844–854. [[CrossRef](#)]
35. Pataky, M.W.; Young, W.F.; Nair, K.S. Hormonal and Metabolic Changes of Aging and the Influence of Lifestyle Modifications. *Mayo Clin. Proc.* **2021**, *96*, 788–814. [[CrossRef](#)]
36. Klein, S.L.; Flanagan, K.L. Sex differences in immune responses. *Nat. Rev. Immunol.* **2016**, *16*, 626–638. [[CrossRef](#)]
37. Diaz Diaz, A.C.; Malone, K.; Shearer, J.A.; Moore, A.C.; Waeber, C. Preclinical Evaluation of Fingolimod in Rodent Models of Stroke With Age or Atherosclerosis as Comorbidities. *Front. Pharmacol.* **2022**, *13*, 920449. [[CrossRef](#)]
38. Bascuñana, P.; Brackhan, M.; Pahnke, J. Machine learning-supported analyses improve quantitative histological assessments of amyloid- $\beta$  deposits and activated microglia. *J. Alzheimer's Dis.* **2021**, *79*, 597–605. [[CrossRef](#)]
39. Singh, S.K.; Kordula, T.; Spiegel, S. Neuronal contact upregulates astrocytic sphingosine-1-phosphate receptor 1 to coordinate astrocyte-neuron cross communication. *Glia* **2022**, *70*, 712–727. [[CrossRef](#)]

40. Dusaban, S.S.; Chun, J.; Rosen, H.; Purcell, N.H.; Brown, J.H. Sphingosine 1-phosphate receptor 3 and RhoA signaling mediate inflammatory gene expression in astrocytes. *J. Neuroinflammation* **2017**, *14*, 111. [[CrossRef](#)] [[PubMed](#)]
41. Spampinato, S.F.; Obermeier, B.; Coteleur, A.; Love, A.; Takeshita, Y.; Sano, Y.; Kanda, T.; Ransohoff, R.M. Sphingosine 1 Phosphate at the Blood Brain Barrier: Can the Modulation of S1P Receptor 1 Influence the Response of Endothelial Cells and Astrocytes to Inflammatory Stimuli? *PLoS ONE* **2015**, *10*, e0133392. [[CrossRef](#)]
42. O'Sullivan, S.A.; O'Sullivan, C.; Healy, L.M.; Dev, K.K.; Sheridan, G.K. Sphingosine 1-phosphate receptors regulate TLR4-induced CXCL5 release from astrocytes and microglia. *J. Neurochem.* **2018**, *144*, 736–747. [[CrossRef](#)]
43. Di Pardo, A.; Amico, E.; Favellato, M.; Castrataro, R.; Fucile, S.; Squitieri, F.; Maglione, V. FTY720 (fingolimod) is a neuroprotective and disease-modifying agent in cellular and mouse models of Huntington disease. *Hum. Mol. Genet.* **2014**, *23*, 2251–2265. [[CrossRef](#)]
44. Miguez, A.; Garcia-Diaz Barriga, G.; Brito, V.; Straccia, M.; Giralt, A.; Gines, S.; Canals, J.M.; Alberch, J. Fingolimod (FTY720) enhances hippocampal synaptic plasticity and memory in Huntington's disease by preventing p75NTR up-regulation and astrocyte-mediated inflammation. *Hum. Mol. Genet.* **2015**, *24*, 4958–4970. [[CrossRef](#)]
45. Vidal-Martinez, G.; Najera, K.; Miranda, J.D.; Gil-Tomme, C.; Yang, B.; Vargas-Medrano, J.; Diaz-Pacheco, V.; Perez, R.G. FTY720 Improves Behavior, Increases Brain Derived Neurotrophic Factor Levels and Reduces alpha-Synuclein Pathology in Parkinsonian GM2+/- Mice. *Neuroscience* **2019**, *411*, 1–10. [[CrossRef](#)]
46. Vidal-Martinez, G.; Vargas-Medrano, J.; Gil-Tomme, C.; Medina, D.; Garza, N.T.; Yang, B.; Segura-Ulate, I.; Dominguez, S.J.; Perez, R.G. FTY720/Fingolimod Reduces Synucleinopathy and Improves Gut Motility in A53T Mice: CONTRIBUTIONS OF PRO-BRAIN-DERIVED NEUROTROPHIC FACTOR (PRO-BDNF) AND MATURE BDNF. *J. Biol. Chem.* **2016**, *291*, 20811–20821. [[CrossRef](#)]
47. Ren, M.; Han, M.; Wei, X.; Guo, Y.; Shi, H.; Zhang, X.; Perez, R.G.; Lou, H. FTY720 Attenuates 6-OHDA-Associated Dopaminergic Degeneration in Cellular and Mouse Parkinsonian Models. *Neurochem. Res.* **2017**, *42*, 686–696. [[CrossRef](#)] [[PubMed](#)]
48. Borchelt, D.R.; Ratovitski, T.; van Lare, J.; Lee, M.K.; Gonzales, V.; Jenkins, N.A.; Copeland, N.G.; Price, D.L.; Sisodia, S.S. Accelerated amyloid deposition in the brains of transgenic mice coexpressing mutant presenilin 1 and amyloid precursor proteins. *Neuron* **1997**, *19*, 939–945. [[CrossRef](#)]
49. Szapacs, M.E.; Numis, A.L.; Andrews, A.M. Late onset loss of hippocampal 5-HT and NE is accompanied by increases in BDNF protein expression in mice co-expressing mutant APP and PS1. *Neurobiol. Dis.* **2004**, *16*, 572–580. [[CrossRef](#)]
50. Radde, R.; Bolmont, T.; Kaeser, S.A.; Coomaraswamy, J.; Lindau, D.; Stoltze, L.; Calhoun, M.E.; Jaggi, F.; Wolburg, H.; Gengler, S.; et al. Abeta42-driven cerebral amyloidosis in transgenic mice reveals early and robust pathology. *EMBO Rep.* **2006**, *7*, 940–946. [[CrossRef](#)] [[PubMed](#)]
51. Mohle, L.; Brackhan, M.; Bascunana, P.; Pahnke, J. Dimethyl fumarate does not mitigate cognitive decline and beta-amyloidosis in female APPS1 mice. *Brain Res.* **2021**, *1768*, 147579. [[CrossRef](#)]
52. Rai, S.P.; Krohn, M.; Pahnke, J. Early Cognitive Training Rescues Remote Spatial Memory but Reduces Cognitive Flexibility in Alzheimer's Disease Mice. *J. Alzheimers Dis.* **2020**, *75*, 1301–1317. [[CrossRef](#)]
53. Rai, S.P.; Bascunana, P.; Brackhan, M.; Krohn, M.; Mohle, L.; Paarmann, K.; Pahnke, J. Detection and Prediction of Mild Cognitive Impairment in Alzheimer's Disease Mice. *J. Alzheimers Dis.* **2020**, *77*, 1209–1221. [[CrossRef](#)]
54. Paarmann, K.; Prakash, S.R.; Krohn, M.; Mohle, L.; Brackhan, M.; Bruning, T.; Eiriz, I.; Pahnke, J. French maritime pine bark treatment decelerates plaque development and improves spatial memory in Alzheimer's disease mice. *Phytomed. Int. J. Phytother. Phytopharm.* **2019**, *57*, 39–48. [[CrossRef](#)]
55. Brackhan, M.; Calza, G.; Lundgren, K.; Bascunana, P.; Bruning, T.; Soliymani, R.; Kumar, R.; Abelein, A.; Baumann, M.; Lalowski, M.; et al. Isotope-labeled amyloid beta does not transmit to the brain in a prion-like manner after peripheral administration. *EMBO Rep.* **2022**, *23*, e54405. [[CrossRef](#)]
56. Mohle, L.; Bascunana, P.; Brackhan, M.; Pahnke, J. Development of deep learning models for microglia analyses in brain tissue using DeePathology STUDIO. *J. Neurosci. Methods* **2021**, *364*, 109371. [[CrossRef](#)]
57. Upite, J.; Bruning, T.; Mohle, L.; Brackhan, M.; Bascunana, P.; Jansone, B.; Pahnke, J. A New Tool for the Analysis of the Effect of Intracerebrally Injected Anti-Amyloid beta Amyloid beta Compounds. *J. Alzheimers Dis.* **2021**, *84*, 1677–1690. [[CrossRef](#)]
58. Steffen, J.; Krohn, M.; Schwitlick, C.; Bruning, T.; Paarmann, K.; Pietrzik, C.U.; Biverstal, H.; Jansone, B.; Langer, O.; Pahnke, J. Expression of endogenous mouse APP modulates beta-amyloid deposition in hAPP transgenic mice. *Acta Neuropathol. Commun.* **2017**, *5*, 49. [[CrossRef](#)]
59. Steffen, J.; Krohn, M.; Paarmann, K.; Schwitlick, C.; Bruning, T.; Marreiros, R.; Muller-Schiffmann, A.; Korth, C.; Braun, K.; Pahnke, J. Revisiting rodent models: Octodon degus as Alzheimer's disease model? *Acta Neuropathol. Commun.* **2016**, *4*, 91. [[CrossRef](#)]

60. Krohn, M.; Bracke, A.; Avchalumov, Y.; Schumacher, T.; Hofrichter, J.; Paarmann, K.; Frohlich, C.; Lange, C.; Bruning, T.; von Bohlen Und Halbach, O.; et al. Accumulation of murine amyloid betaamyloid beta mimics early Alzheimer's disease. *Brain* **2015**, *138 Pt 8*, 2370–2382. [[CrossRef](#)] [[PubMed](#)]
61. Wu, J.; Möhle, L.; Brüning, T.; Eiriz, I.; Rafehi, M.; Stefan, K.; Stefan, S.M.; Pahnke, J. A Novel Huntington's Disease Assessment Platform to Support Future Drug Discovery and Development. *Int. J. Mol. Sci.* **2022**, *23*, 14763. [[CrossRef](#)] [[PubMed](#)]

**Disclaimer/Publisher's Note:** The statements, opinions and data contained in all publications are solely those of the individual author(s) and contributor(s) and not of MDPI and/or the editor(s). MDPI and/or the editor(s) disclaim responsibility for any injury to people or property resulting from any ideas, methods, instructions or products referred to in the content.